Causal Mechanical Cosmology (CMC) — Paper 5

A Word-Safe Mathematical Derivation Tooling Paper for A–B–C Closure

Dipole/Quadrupole LOS Signatures and Atomic Frequency-Shift Observable Anchoring

Author: Léon Barbour
ORCID: 0009-0001-0174-4672
Email: leonbarbour@googlemail.com
Date: 2026-02-06

Abstract

This paper presents a compact "tooling derivation" for the first closed operational loop in Causal Mechanical Cosmology (CMC): (A) spherical void control geometry producing a dominant dipole anisotropy for an off-centre observer, (B) an elongated/sheared void geometry producing quadrupole anisotropy via a local Hessian decomposition, and (C) an observable closure mapping the structural line-of-sight (LOS) velocity signature to atomic fractional frequency shift $\Delta f/f$ as the measurement endpoint. Canonical equations (E1–E8) are preserved and used as the spine for derivations and diagnostics.

The local Hessian kernel yields the leading even-parity multipole structure (monopole/quadrupole); dipole structure in the spherical off-centre control case is treated as arising from the global sampling asymmetry and, in a strict local expansion, enters through higher-order terms beyond the first Hessian approximation.

1. Introduction

Large-scale cosmic anisotropies are typically discussed in kinematic and metric terms. CMC instead frames the immediate, falsifiable target as an operational loop: a geometric/structural model produces a concrete LOS velocity signature, and that signature is mapped to an observable frequency shift with an explicit residual term ε capturing unexplained structure.

This paper is a tooling paper In particular, the Hessian approximation is treated as the leading-order even-parity generator of angular structure; any dipole component arising from off-centre geometry is expected to enter through global sampling asymmetry and/or higher-order derivatives beyond the leading Hessian term.

Scope discipline (explicit):

- A–B–C is treated as the first closed operational loop.
- Claims are diagnostic and falsifiable; metaphor is not promoted to ontology without derivation.
- No premature data-fitting claims are made here.

  The purpose of this paper is to establish the closed derivation and diagnostic extraction machinery; real-data sky overlays are explicitly deferred to the subsequent paper.

2. Canonical Definitions and Symbols

The following quantities are defined and used throughout this paper.

- $\Phi(\mathbf{x})$: structural potential field
- $\mathbf{u}(\mathbf{x})$: structural flow / velocity field
- $\mathbf{r}_0$: observer location
- $\hat{n}$: line-of-sight (LOS) unit vector
- d: baseline separation distance along LOS
- $H = \nabla\nabla\Phi$: Hessian of Φ
- S: traceless shear component of Hessian
- K: coupling constant in $\mathbf{u} = -K\nabla\Phi$
- f: atomic transition frequency
- $\frac{\Delta f}{f}$: fractional frequency shift
- ε: unexplained residual structural signal
- c: speed of light
- h: Planck constant

Dimensional convention (explicit):

In this tooling paper, Φ is treated as a structural scalar field whose physical dimension is not fixed a priori. The coupling κ in (E2) is therefore treated as the dimensional conversion constant required to map ∇Φ into a velocity field. Operationally, κ is treated as a calibration parameter determined by matching predicted LOS signatures to measured fractional frequency shifts under (E6–E8). Dimensional closure is therefore enforced at the level of observables rather than imposed at the level of ontology.

3. Canonical Equation Spine (Registry Preserved)

The following canonical equations define the A–B–C operational chain and are treated as locked.

(E1) LOS Differential Velocity Signature

$$u_{\parallel}(d,\hat{n}) = [\mathbf{u}(\mathbf{r}_0 + d\hat{n}) - \mathbf{u}(\mathbf{r}_0)] \cdot \hat{n}$$

(E2) Structural Flow Definition

$$\mathbf{u}(\mathbf{x}) = -K\nabla\Phi(\mathbf{x})$$

(E3) Local Hessian Kernel Approximation

$$u_{\parallel}(d,\hat{n}) \approx -Kd(\hat{n}^T H(\mathbf{r}_0)\hat{n})$$

(E4) Hessian Trace + Traceless Decomposition

$$H = \left(\frac{\mathrm{Tr}(H)}{3}\right) I + S, \mathrm{Tr}(S) = 0$$

(E5) Angular Kernel Decomposition

$$\hat{n}^T H\hat{n} = \frac{\mathrm{Tr}(H)}{3} + \hat{n}^T S\hat{n}$$

(E6) Structural LOS Signature to Frequency Shift Closure

$$\frac{\Delta f}{f} \approx -\frac{u_{\parallel}}{c}$$

(E7) Atomic Frequency Definition

$$f = \frac{\Delta E}{h}$$

(E8) Full Shift Budget with Residual Structural Term

$$\frac{\Delta f}{f} = (\mathrm{GR}) + (\mathrm{Doppler}) + (\mathrm{EM}) + (\mathrm{Thermal}) + (\mathrm{Collisional}) + \varepsilon$$

Validity note: Equations (E1–E8) define the operational diagnostic chain. Where local Taylor expansions are used, the approximation is valid only in the small-baseline regime $D \ll L$, where $L$is the characteristic curvature scale of Φ.

4. Derivation of the Local LOS Kernel (E1 → E3)

This section derives the local angular kernel that generates dipole/quadrupole structure in the small-baseline (local) limit.

4.1 LOS Differential Definition (Primitive Observable Object)

The measured LOS differential velocity along direction $\hat{n}$over baseline distance $d$is defined as:

$$u_{\parallel}(d,\hat{n}) = [u(r_0 + d\hat{n}) - u(r_0)] \cdot \hat{n}$$

This is the fundamental CMC LOS signature used throughout the A–B–C loop.

4.2 Structural Flow Model

CMC assumes the structural flow is generated by the gradient of a structural potential Φ, with coupling constant K:

$$u(x) = -K\nabla\Phi(x)$$

4.3 Local Taylor Expansion of the Flow Field

Assuming $d$is sufficiently small compared to the characteristic curvature scale $L$of Φ, such that $d \ll L$, a local expansion about $r_0$is valid. The expansion is truncated at leading order, with neglected terms $O(d^2)$.

Expand:

$$u(r_0 + d\hat{n}) \approx u(r_0) + d(\nabla u)(r_0)\hat{n}$$

where $(\nabla u)(r_0)$is the local velocity-gradient (Jacobian) tensor.

Then:

$$u(r_0 + d\hat{n}) - u(r_0) \approx d(\nabla u)(r_0)\hat{n}$$

Substitute into (E1):

$$u_{\parallel}(d,\hat{n}) \approx [d(\nabla u)(r_0)\hat{n}] \cdot \hat{n} = d\,\hat{n}^T(\nabla u)(r_0)\hat{n}$$

4.4 Hessian Identification

Using (E2):

$$\nabla u = -K\nabla(\nabla\Phi) = -K\nabla\nabla\Phi = -KH$$

Thus:

$$u_{\parallel}(d,\hat{n}) \approx -Kd(\hat{n}^T H(r_0)\hat{n})$$

The angular response kernel is therefore:

$$Q(\hat{n}) = \hat{n}^T H(r_0)\hat{n}$$

This kernel is the local mathematical generator of anisotropy. Since $Q(\hat{n})$is even under $\hat{n} \to -\hat{n}$, the leading-order Hessian kernel generates even-parity multipoles (monopole/quadrupole). Dipole structure requires higher-order terms or global off-centre sampling effects.

5. Hessian Decomposition and the Origin of Dipole vs Quadrupole (E4 → E5)

This section shows how isotropic curvature and anisotropic shear split cleanly, and why quadrupole structure emerges naturally.

5.1 Trace + Traceless Tensor Decomposition

The Hessian is decomposed into an isotropic trace term plus a traceless shear term:

$$H = \frac{\mathrm{Tr}(H)}{3} I + S, \mathrm{Tr}(S) = 0$$

5.2 Quadratic Angular Response Decomposition

Insert (E4) into the quadratic form:

$$\hat{n}^T H\hat{n} = \hat{n}^T \left[\frac{\mathrm{Tr}(H)}{3} I + S\right]\hat{n} = \frac{\mathrm{Tr}(H)}{3}\hat{n}^T I\hat{n} + \hat{n}^T S\hat{n}$$

Since $\hat{n}^T I\hat{n} = 1$:

$$\hat{n}^T H\hat{n} = \frac{\mathrm{Tr}(H)}{3} + \hat{n}^T S\hat{n}$$

5.3 Operational Interpretation

- $\frac{\mathrm{Tr}(H)}{3}$ contributes an angularly constant monopole component.
- $\hat{n}^T S \hat{n}$ contributes the anisotropic quadrupole structure.

Because S is traceless, this anisotropic term contains no monopole contribution. Thus, quadrupole anisotropy is mathematically tied to the traceless shear tensor S. Operationally, this means that persistent $\ell = 2$ structure is a direct diagnostic of non-zero shear tensor S_{ij} in the local structural Hessian.

6. Section A — Spherical Void Control: Dipole-Dominant Anisotropy from Off-Centre Observer

This section defines the spherical control geometry and explains why the predicted anisotropy is dominantly dipolar.

6.1 Control Geometry Definition

Consider a spherical void-like region (KBC-like control structure) with radial symmetry about a centre point C. The structural potential Φis spherically symmetric about C, but the observer is displaced such that:

$$r_0 \neq C$$

6.2 Why a Dipole Appears

Even in a perfectly spherical void, an off-centre observer does not sample the structure symmetrically across the sky. The LOS signature $u_{\parallel}(d, \hat{n})$ therefore becomes directionally biased, producing a dipolar sky signature aligned with the displacement axis.

This is a geometric effect: it does not require intrinsic shear.

Dipole mechanism note (local vs global):
In the strict leading-order Hessian truncation of Section 4, the kernel is even-parity and does not generate a true $\ell = 1$term by itself. The dipole associated with the spherical off-centre control geometry is therefore interpreted as a global sampling asymmetry of the spherical profile, and in a strict derivative expansion is expected to enter through spatial variation of the Hessian along the LOS (higher-order derivatives of Φ). This paper treats the spherical off-centre dipole as a control prediction of the full geometry rather than as a claim derived solely from the leading Hessian term.

6.3 Control-Axis Prediction (Dipole Alignment Condition)

In the spherical control geometry, the predicted dipole axis is aligned with the observer displacement vector:

$$\Delta r = r_0 - C$$

i.e. the direction from the void centre Ctoward the observer position r_0.

The dipole should remain stable in direction as d varies, subject only to measurement noise and higher-order corrections beyond the local approximation.

6.4 Why Quadrupole is Suppressed in the Ideal Spherical Control

In the spherical ideal limit, the traceless shear component $S$is zero or cancels under symmetry, leaving only isotropic curvature contributions. Thus, persistent quadrupole structure is expected to be suppressed in the ideal spherical control limit, with any residual quadrupole arising from departures from perfect symmetry, environmental structure, or higher-order corrections beyond the local truncation. Therefore, detection of a strong stable quadrupole component in the spherical control case would indicate either non-sphericity, external structure, or breakdown of the ideal control assumptions.

CMC A-claim (bounded):
Spherical void + off-centre observer → dipole-dominant anisotropy signature, with quadrupole suppressed in the ideal spherical symmetry limit.

7. Section B — Elongated Void Case: Quadrupole from Traceless Shear *S*

This section introduces intrinsic elongation/shear, which generates quadrupole structure.

7.1 Elongation as a Shear-Generating Deformation

An elongated void can be modelled as a departure from spherical symmetry such that the local Hessian contains a non-zero traceless component:

$$S \neq 0$$

This shear tensor represents intrinsic directional deformation of the structure.

7.2 Quadrupole Emergence Directly from the Kernel

From (E3):

$$u_{\parallel}(d,\hat{n}) \approx -Kd(\hat{n}^T H \hat{n})$$

Insert (E5):

$$u_{\parallel}(d,\hat{n}) \approx -Kd\left[\frac{\mathrm{Tr}(H)}{3} + \hat{n}^T S \hat{n}\right]$$

Thus:

- The trace term is isotropic.
- The shear term is anisotropic and quadrupolar.
- Therefore, the quadrupole amplitude is expected to scale linearly with baseline $d$in the local regime, until higher-order corrections dominate.

CMC B-claim (bounded):
Elongated/sheared void → quadrupole anisotropy generated by traceless shear S.

7.3 Eigenstructure Interpretation (Operational)

The principal axes of the quadrupole correspond to the eigenvectors of S. Therefore, a measured quadrupole axis that is unstable with baseline d, or inconsistent with the inferred shear axis, would directly falsify the elongated void interpretation.

8. Multipole Extraction Diagnostics (A_1, A_2, Axis Alignment)

This section defines how dipole and quadrupole amplitudes are extracted from predicted or observed sky maps.

8.1 Full-Sky LOS Map as the Primitive Diagnostic Object

For each baseline d, define the full-sky scalar field:

$$U_d(\hat{n}) \equiv u_{\parallel}(d,\hat{n})$$

This is the predicted or inferred LOS differential velocity field on the sphere.

8.2 Dipole and Quadrupole Amplitudes

Define:

- $A_1(d)$ as the extracted dipole amplitude ($\ell = 1$)
- $A_2(d)$ as the extracted quadrupole amplitude ($\ell = 2$)

These are obtained via spherical-harmonic decomposition, or equivalently via least-squares projection onto the $\ell = 1$and $\ell = 2$ basis functions.

For observational data with incomplete sky coverage or masking, the extracted multipoles must be treated as pseudo-multipoles unless a reconstruction method is applied. This paper assumes full-sky synthetic benchmarks as the validation baseline.

Operationally, $A_\ell(d)$ may be reported either as total harmonic power $\sum_m | a_{\ell m}(d) |^2$ or as RMS amplitude, provided the convention is held fixed across datasets.

8.3 Normalization Convention (Explicit; Word-Safe)

For consistency across synthetic benchmarks and future observational overlays, the multipole amplitudes $A_1(d)$and $A_2(d)$ are defined using the standard orthonormal spherical-harmonic convention:

$$\int_{S^2} Y_{\ell m}(\hat{n})\, Y^*_{\ell' m'}(\hat{n})\, d\Omega = \delta_{\ell\ell'}\delta_{mm'}$$

Under this convention, the extracted amplitude at each ℓ is treated as the RMS harmonic power contribution of that ℓ-mode to the full-sky field $U_d(\hat{n})$, enabling direct cross-comparison of dipole and quadrupole strength as a function of baseline d.

8.4 Axis Alignment Diagnostics

For each baseline d, compute:

- Dipole axis: best-fit $\ell = 1$ direction vector
- Quadrupole principal axes: best-fit $\ell = 2$ tensor eigenvectors (or equivalently inferred from S)

Then define alignment measures such as:

- angular separation between dipole axis and displacement axis Δr
- angular separation between quadrupole principal axis and the elongation/shear axis

These provide falsifiable predictions: amplitude and axis must both match.

9. Section C — Observable Closure: Mapping $u_{\parallel}$ to Atomic Frequency Shift (E6–E8)

This section closes the A–B–C loop by mapping the LOS structural signature into a measurable atomic frequency shift.

9.1 Frequency as the Operational Observable Endpoint

Atomic transition frequency is defined by:

$$f = \frac{\Delta E}{h}$$

CMC treats frequency as the measurement anchor because it is experimentally accessible at extreme precision.

9.2 LOS Structural Signature to Fractional Frequency Shift Mapping

The operational closure mapping is:

$$\frac{\Delta f}{f} \approx -\frac{u_{\parallel}}{c}$$

Operationally, d corresponds to the separation scale associated with the LOS differential comparison, such as two clock locations connected by a stabilized link, or an effective differential sampling length scale in a sky survey proxy observable.

Thus, for each baseline d, the predicted LOS sky field $U_d(\hat{n})$ corresponds to a predicted fractional frequency shift sky field:

$$\left(\frac{\Delta f}{f}\right)_d (\hat{n}) \approx -\frac{U_d(\hat{n})}{c}$$

Equation (E6) is treated as a first-order operational mapping consistent with the non-relativistic Doppler approximation $| v | \ll c$. Higher-order relativistic corrections may be included if required, but are not needed for the first A–B–C closure demonstration. This closure is treated as an operational measurement mapping rather than a claim that all contributions to $\frac{\Delta f}{f}$ are purely kinematic.

9.3 Shift Budget Closure and Residual Structural Term

In real clock comparisons, the fractional shift is the sum of known contributions plus an unexplained residual:

$$\frac{\Delta f}{f} = (\mathrm{GR}) + (\mathrm{Doppler}) + (\mathrm{EM}) + (\mathrm{Thermal}) + (\mathrm{Collisional}) + \epsilon$$

Here, $\epsilon = \epsilon(\hat{n}, d)$represents the residual structural signal after known corrections are applied. In principle, $\epsilon(\hat{n}, d)$may itself be decomposed into spherical harmonics, allowing direct tests of whether residual structure is dominantly dipolar, quadrupolar, or higher-order.

CMC therefore defines a disciplined falsifiability channel: any claimed cosmological structural effect must appear in ϵafter transparent subtraction of known contributions.

10. Synthetic Benchmarks and Figure Suite (Pipeline Validation Framework)

This tooling paper assumes a synthetic benchmark suite exists to validate the pipeline end-to-end before applying observational datasets.

The benchmark suite includes:

- $u_{\parallel}(d, \hat{n})$ full-sky maps
- $\frac{\Delta f}{f}$ full-sky maps
- extracted dipole amplitude $A_1(d)$vs $\frac{d}{R}$
- extracted quadrupole amplitude $A_2(d)$vs $\frac{d}{R}$
- dipole axis alignment vs d
- quadrupole axis alignment vs d

11. Discussion (Bounded Interpretation)

11.1 What Paper 5 Establishes

Paper 5 establishes a minimal closed operational chain:

- A structural potential Φ generates flow $u$via (E2).
- The LOS differential signature $u_{\parallel}(d, \hat{n})$ is defined by (E1).
- In the local approximation, $u_{\parallel}$reduces to the Hessian kernel (E3).
- Decomposition (E4–E5) separates isotropic curvature from shear anisotropy.

- Dipole and quadrupole components are extracted with explicit multipole normalization.
- The LOS structural signature maps to atomic fractional frequency shift via (E6–E8).

This yields a reproducible diagnostic pipeline: geometry → anisotropy → observable closure.

The result is not a full cosmological solution; it is a controlled forward model producing multipole-predictive signatures that can be benchmarked synthetically and then confronted with observational residual maps.

11.2 Dark-Sector Mapping (Interpretation Only; Not Claimed as Proof)

CMC maintains a provisional interpretive mapping in which the background medium behaves analogously to an order-supporting component (dark matter proxy), while excitation/expansion modes behave analogously to a dispersive pressure component (dark energy proxy). This paper does not claim proof of this mapping and treats it strictly as interpretation pending survival of falsifiable A–B–C tests.

11.3 Limitations

- The Hessian approximation in (E3) is a local expansion; higher-order corrections may be required for large baselines.
- Multipole extraction must be applied consistently when masks or incomplete sky coverage exist in observational data.
- The closure relation (E6) is operational; it defines measurement mapping rather than a full cosmological model fit.
- In particular, dipole structure in the spherical off-centre case is treated as a global geometric control prediction; strict dipole emergence may require inclusion of higher-order derivative terms beyond the leading Hessian truncation.

12. Conclusion

This paper provides the mathematical tooling for CMC's first closed operational loop A–B–C: dipole-dominant anisotropy in a spherical control geometry for an off-centre observer, quadrupole anisotropy generated by traceless shear in an elongated geometry, and an observable closure mapping LOS structural signatures into fractional atomic frequency shifts with an explicit residual term ϵ.

The result is a compact Word-safe derivation and diagnostic framework suitable for synthetic benchmark validation and subsequent overlay onto observational datasets without premature claims.

Appendix A — Equation Registry (E1–E8, Unchanged)

(E1) LOS Differential Velocity Signature

$$u_{\parallel}(d,\hat{n}) = [u(r_0 + d\hat{n}) - u(r_0)] \cdot \hat{n}$$

(E2) Structural Flow Definition

$$u(x) = -K\nabla\Phi(x)$$

(E3) Local Hessian Kernel Approximation

$$u_{\parallel}(d,\hat{n}) \approx -Kd(\hat{n}^T H(r_0)\hat{n})$$

(E4) Hessian Trace + Traceless Decomposition

$$H = \frac{\mathrm{Tr}(H)}{3} I + S, \mathrm{Tr}(S) = 0$$

(E5) Angular Kernel Decomposition

$$\hat{n}^T H \hat{n} = \frac{\mathrm{Tr}(H)}{3} + \hat{n}^T S \hat{n}$$

(E6) Structural LOS Signature to Frequency Shift Closure

$$\frac{\Delta f}{f} \approx -\frac{u_{\parallel}}{c}$$

(E7) Atomic Frequency Definition

$$f = \frac{\Delta E}{h}$$

(E8) Full Shift Budget with Residual Structural Term

$$\frac{\Delta f}{f} = (\mathrm{GR}) + (\mathrm{Doppler}) + (\mathrm{EM}) + (\mathrm{Thermal}) + (\mathrm{Collisional}) + \epsilon$$

Appendix B — Symbol Table (Canonical)

Symbol	Meaning
$\Phi(\mathbf{x})$	structural potential
$\mathbf{u}(\mathbf{x})$	structural flow field
$\mathbf{r}_0$	observer location
$\hat{n}$	LOS unit vector
d	baseline separation
H	Hessian $\nabla\nabla\Phi$
S	traceless shear tensor
K	coupling constant
f	atomic transition frequency
$\frac{\Delta f}{f}$	fractional frequency shift
c	speed of light
h	Planck constant
ε	unexplained residual term

Appendix C — Figure Index and Placement Map

FIGURE 1: Spherical void — centred observer (monopole control)
FIGURE 2: Spherical void — off-centre observer (dipole signature)
FIGURE 3: Elongated void — centred observer (quadrupole signature)
FIGURE 4: Elongated void — off-centre observer (dipole + quadrupole)
FIGURE 5: $\frac{\Delta f}{f}$map — spherical off-centre
FIGURE 6: $\frac{\Delta f}{f}$map — elongated/sheared
FIGURE 7: Dipole amplitude $A_1(d)$scaling curve
FIGURE 8: Quadrupole amplitude $A_2(d)$scaling curve
FIGURE 9: Dipole axis alignment vs baseline d
FIGURE 10: Quadrupole axis alignment vs baseline d

Appendix D — Example Spherical Structural Potential (Toy Control Model)

Consider a spherical structural potential of the form

$$\Phi(r) = \Phi_0 \exp\left(\quad -\frac{r^2}{R^2} \right)$$

where $r = | \mathbf{r} - \mathbf{r}_c |$ is distance from the void centre.

The gradient and Hessian of Φ are well-defined and yield an isotropic trace-dominant curvature structure when evaluated at the symmetry centre. Departures from centre sampling introduce directional asymmetry through spatial variation of derivatives along the LOS.This toy form is provided only to demonstrate that the control geometry is mathematically constructible, not as a claim of physical uniqueness.

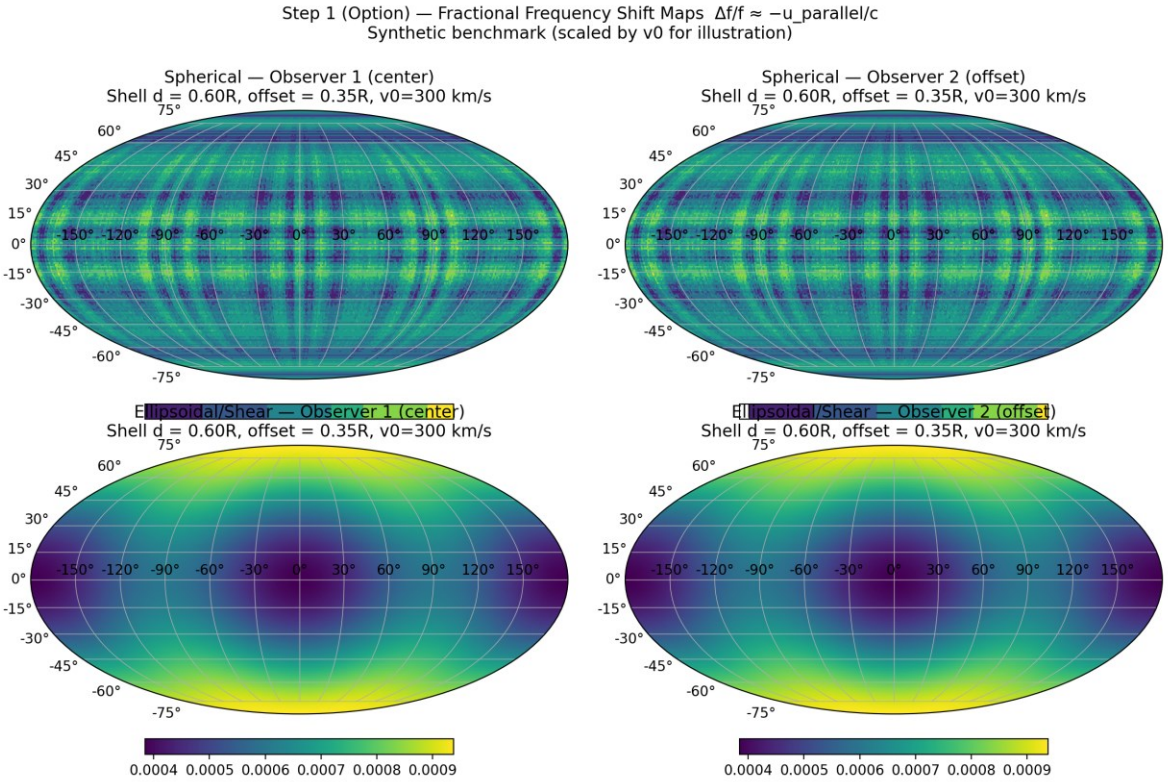
Step 1 (Option) — Fractional Frequency Shift Maps Δf/f ≈ −u_parallel/c
Synthetic benchmark (scaled by v0 for illustration)
Spherical — Observer 1 (center)
Shell d = 0.60R, offset = 0.35R, v0=300 km/s
Spherical — Observer 2 (offset)
Shell d = 0.60R, offset = 0.35R, v0=300 km/s
Ellipsoidal/Shear — Observer 1 (center)
Shell d = 0.60R, offset = 0.35R, v0=300 km/s
Ellipsoidal/Shear — Observer 2 (offset)
Shell d = 0.60R, offset = 0.35R, v0=300 km/s
0.0004 0.0005 0.0006 0.0007 0.0008 0.0009

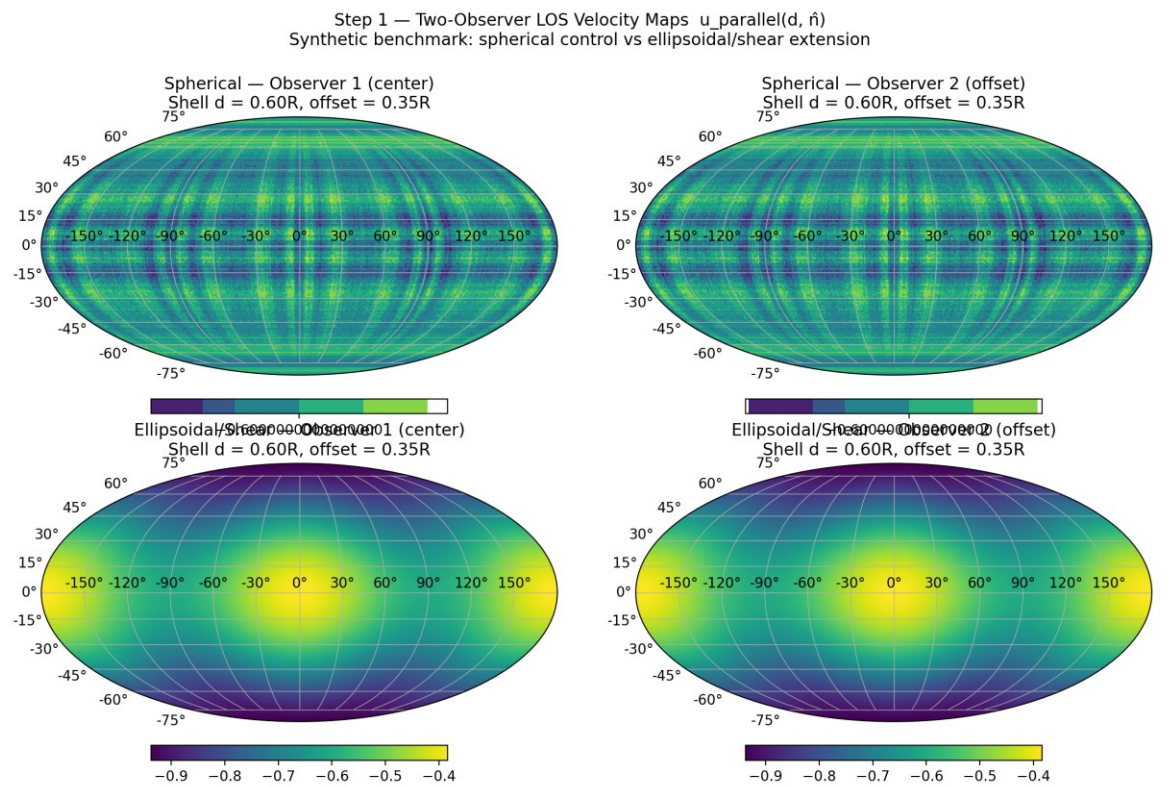
Step 1 — Two-Observer LOS Velocity Maps u_parallel(d, n̂)
Synthetic benchmark: spherical control vs ellipsoidal/shear extension
Spherical — Observer 1 (center)
Shell d = 0.60R, offset = 0.35R
Spherical — Observer 2 (offset)
Shell d = 0.60R, offset = 0.35R
Ellipsoidal/Shear — Observer 1 (center)
Shell d = 0.60R, offset = 0.35R
Ellipsoidal/Shear — Observer 2 (offset)
Shell d = 0.60R, offset = 0.35R
−0.9 −0.8 −0.7 −0.6 −0.5 −0.4

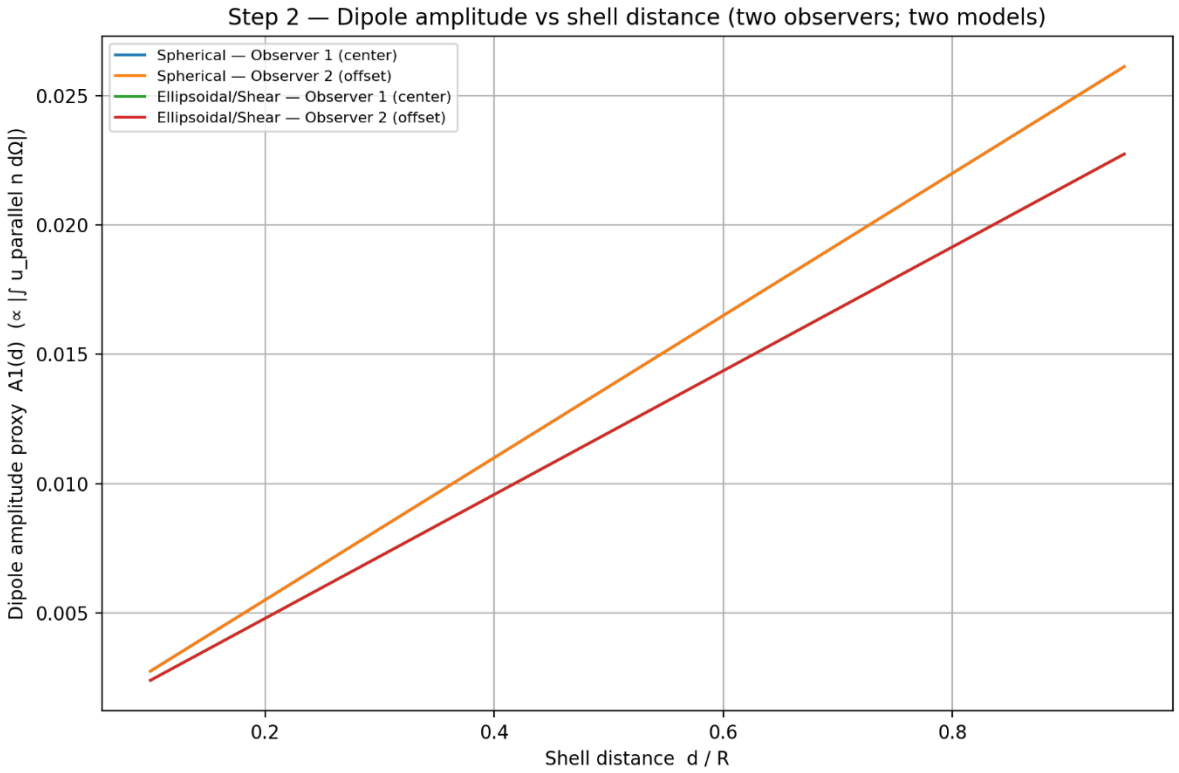
Step 2 — Dipole amplitude vs shell distance (two observers; two models)
Spherical — Observer 1 (center)
Spherical — Observer 2 (offset)
Ellipsoidal/Shear — Observer 1 (center)
Ellipsoidal/Shear — Observer 2 (offset)
Dipole amplitude proxy A1(d) (∝ |∫ u_parallel n dΩ|)
0.025
0.020
0.015
0.010
0.005
0.2
0.4
0.6
0.8
Shell distance d / R

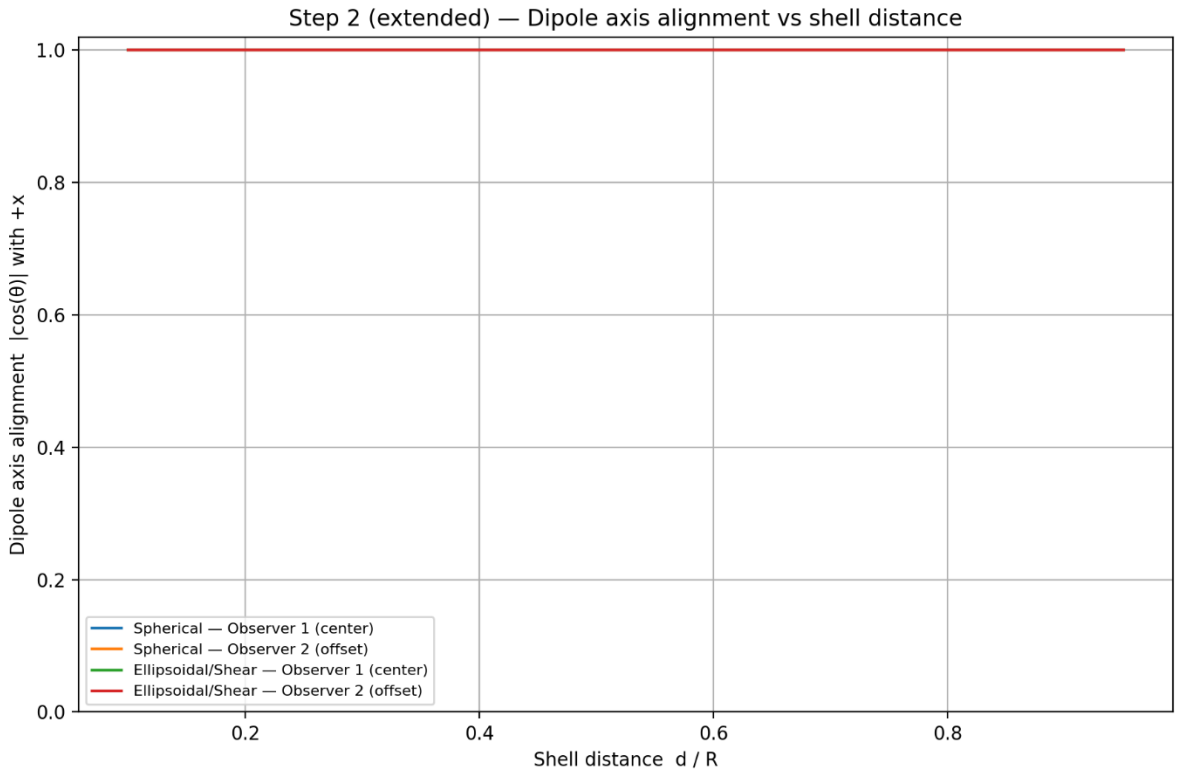
Step 2 (extended) — Dipole axis alignment vs shell distance
Dipole axis alignment |cos(θ)| with +x
1.0
0.8
0.6
0.4
0.2
0.0
Spherical — Observer 1 (center)
Spherical — Observer 2 (offset)
Ellipsoidal/Shear — Observer 1 (center)
Ellipsoidal/Shear — Observer 2 (offset)
0.2
0.4
0.6
0.8
Shell distance d / R

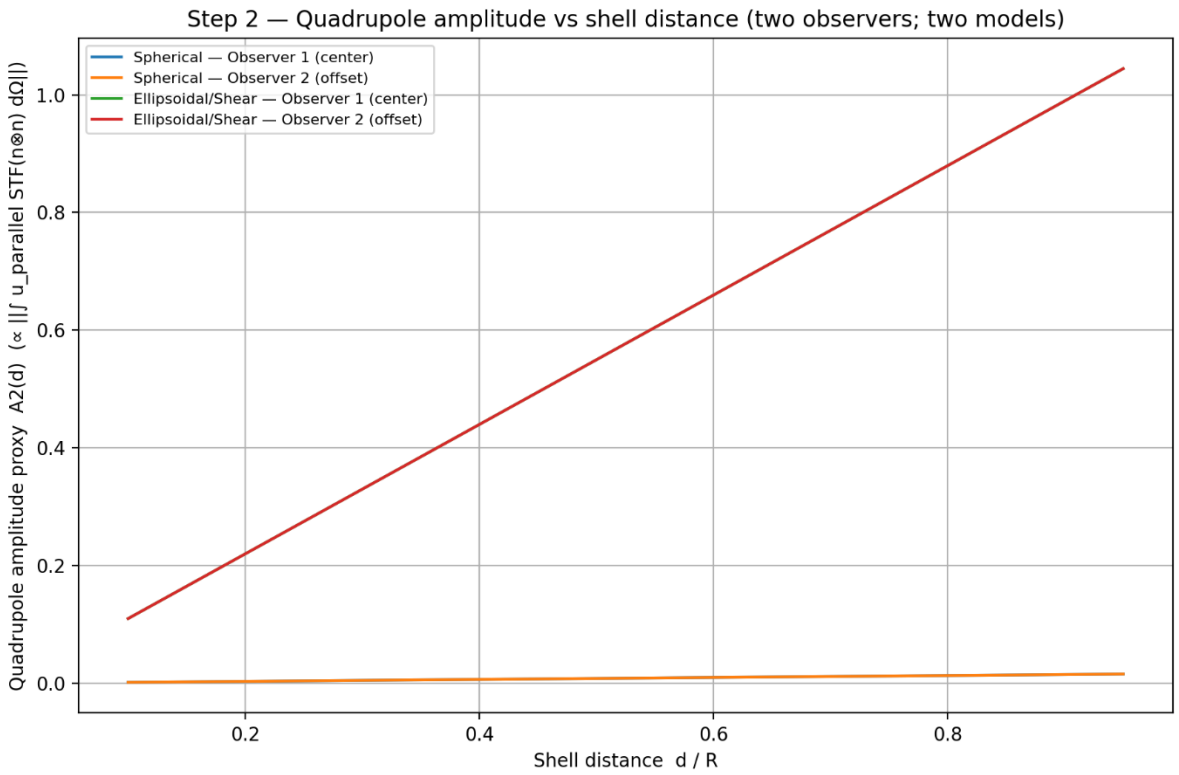
Step 2 — Quadrupole amplitude vs shell distance (two observers; two models)
Spherical — Observer 1 (center)
Spherical — Observer 2 (offset)
Ellipsoidal/Shear — Observer 1 (center)
Ellipsoidal/Shear — Observer 2 (offset)
Quadrupole amplitude proxy A2(d) (∝ ||∫ u_parallel STF(n⊗n) dΩ||)
0.0
0.2
0.4
0.6
0.8
1.0
0.2
0.4
0.6
0.8
Shell distance d / R

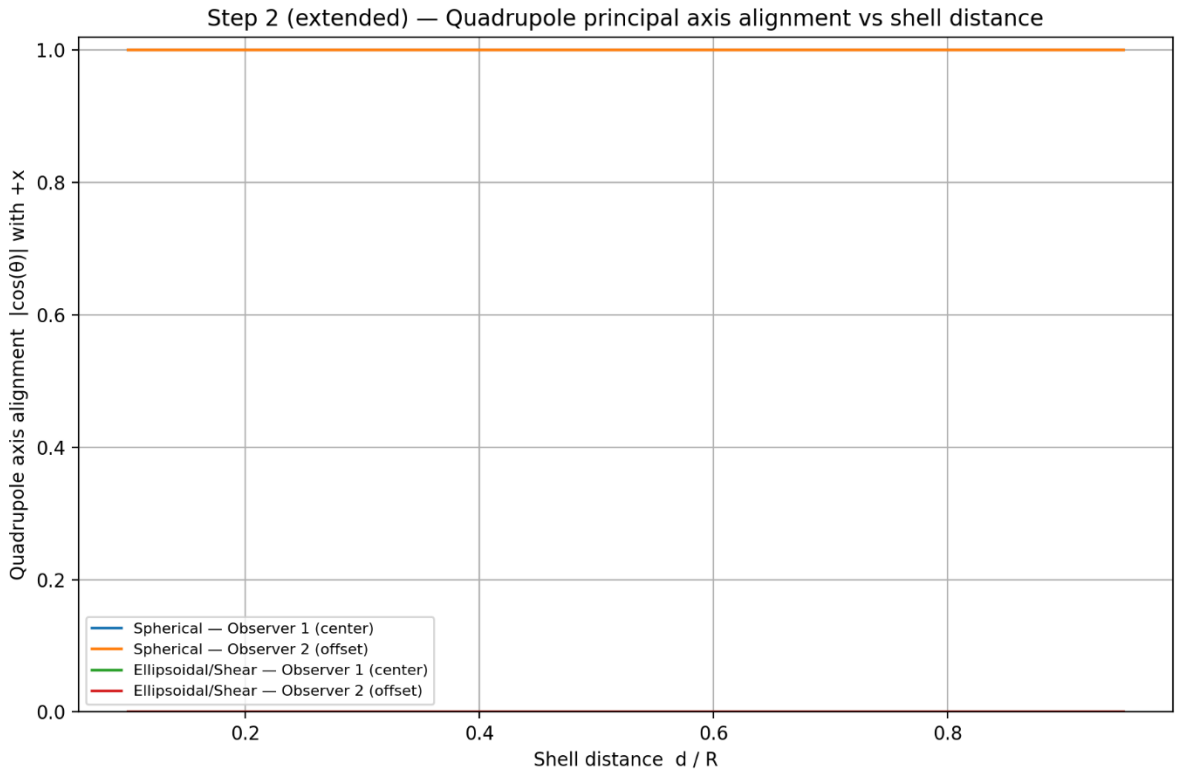
Step 2 (extended) — Quadrupole principal axis alignment vs shell distance
Spherical — Observer 1 (center)
Spherical — Observer 2 (offset)
Ellipsoidal/Shear — Observer 1 (center)
Ellipsoidal/Shear — Observer 2 (offset)
Quadrupole axis alignment |cos(θ)| with +x
0.0
0.2
0.4
0.6
0.8
1.0
0.2
0.4
0.6
0.8
Shell distance d / R

Final Administrative & Compliance Statements

Conflict of Interest: The author declares no conflicts of interest.

Funding: This research received no external funding and was conducted independently by the author.

Author Contributions: All conceptual development, causal reasoning, mathematical formulation, derivations, analysis, interpretation, and manuscript preparation were performed solely by the author.

AI-Use Disclosure: Artificial-intelligence tools were used exclusively for translation assistance, clerical organization, and general research support. AI systems did not generate, modify, select, or validate any scientific ideas, derivations, theoretical constructs, or conclusions. All scientific direction, reasoning, and insight originate entirely from the author.

Data Availability: No empirical datasets were used in this study. Synthetic benchmark materials referenced in the text will be released in a subsequent companion paper or provided upon reasonable request.

Acknowledgements: The author acknowledges the use of standard computational and document-processing tools during manuscript preparation. All scientific insight and methodological development remain the sole work of the author.

Programme & Licensing:
Causal Mechanical Cosmology (CMC) Independent Research Programme

Author Identifiers:
ORCID: 0009-0001-0174-4672
Email: leonbarbour@googlemail.com